



Full paper

Manipulating electrolyte and solid electrolyte interphase to enable safe and efficient Li-S batteries

Jing Zheng^{a,b,1}, Xiulin Fan^{a,1}, Guangbin Ji^b, Haiyang Wang^a, Singyuk Hou^a, Kerry C. DeMella^c, Srinivasa R. Raghavan^a, Jing Wang^d, Kang Xu^e, Chunsheng Wang^{a,*}

^a Department of Chemical and Biomolecular Engineering University of Maryland, College Park, MD 20742, USA

^b College of Materials Science and Technology, Nanjing University of Aeronautics and Astronautics, Nanjing 210016, PR China

^c Department of Chemistry and Biochemistry, University of Maryland, College Park, MD 20742, USA

^d School of Materials Science and Engineering, Jiamusi University, Jiamusi 154007, PR China

^e Electrochemistry Branch, Power and Energy Division Sensor and Electron Devices Directorate, US Army Research Laboratory, Adelphi, MD 20783, USA

ARTICLE INFO

Keywords:

Lithium-sulfur battery
Shuttle effect
Lithium dendrite
Concentrated electrolyte

ABSTRACT

Li-S batteries have been considered promising candidates for the next-generation energy storage devices because of their extremely high energy densities and low cost. However, Li dendrite formation/dissolution and shuttle of high-order polysulfides prevent their practical applications. Herein, we demonstrate a highly concentrated electrolyte, 12 M lithium bis(fluorosulfonyl)imide (LiFSI) salt in DME solvent (12 M LiFSI/DME), that can effectively suppress both the Li dendritic growth on the anode and the polysulfide shuttle reactions on the cathode side. The highly concentrated electrolyte along with the robust solid electrolyte interphase (SEI) formed therein play the key role in achieving high coulombic efficiencies for both Li stripping/plating (> 99.2%) and S cathode (> 99.7%). Based on the in-depth understanding of the interactions between electrodes and highly concentrated electrolyte, we designed a novel dilute electrolyte (1 M LiFSI/HFE + DME), which achieves similar electrochemical performances in Li-S batteries as the concentrated electrolytes. These Li-S batteries with the highest CE for Li anode and sulfur cathode maintains a high reversible capacity of 786 mA h/g at 0.1 A/g after 300 cycles, or 644 mA h/g at 300th cycle even at 1 A/g without any detectable shuttle reactions.

1. Introduction

Advanced energy storage systems with high energy density, long cycle life and low cost are critical solutions to our future energy demand. Current lithium-ion batteries (LIBs), which have been widely used in portable electronic devices over the past several decades are approaching the energy density ceiling set by the intercalation chemistries and the cost bottom set by transition metal oxides. Within this context, Li-S batteries with much higher energy density due to the conversion-reaction manner of both Li-metal and S and low cost of the latter have drawn intense attention. However, two intrinsic barriers associated with the nature of Li-S chemistry still hinder their practical application: (1) Li dendrite growth which not only induces irreversible electrolyte consumption but also raises safety concern [1]; and (2) the dissolution and subsequent shuttle of high order lithium polysulfide species that causes persistent loss of active sulfur material and low coulombic efficiency [2].

Many approaches have been adopted to suppress the Li dendrite

growth and increase the Li anode CE, the most successful way of which are coating carbon-based interlayers on Li metal anode [3], forming solid-state electrolyte protection layer [4], and manipulating the electrolyte compositions to suppress dissolution of polysulfide species [5]. Due to the relatively lower reactivity of ether on Li metal, ether-based electrolytes with high salt concentration have been extensively investigated for Li-S batteries. Henderson et al. demonstrated that ether-based electrolyte still has considerable ionic conductivity even at a high concentration [6]. Suo et al. reported that the Li dendrite deposition can be suppressed in the highly-concentrated ether electrolyte, although the CE of ~ 74% is still not high enough [7]. Zhang et al. also confirmed that a highly concentrated electrolyte can achieve a high Li CE and suppress Li dendrite [8]. However, high CE and/or free Li dendrite can only be achieved at a low current density [3a,9]; and superior electrochemical performance of ether-based electrolytes can only sustain for limited cycles owing to the less reactive of the reduction product (LiOH, Li₂O and so on) on the Li surface [9]. On the other hand, considerable efforts on reformulating electrolytes in order to suppress

* Corresponding author.

E-mail address: cswang@umd.edu (C. Wang).

¹ These authors contributed equally to this work.

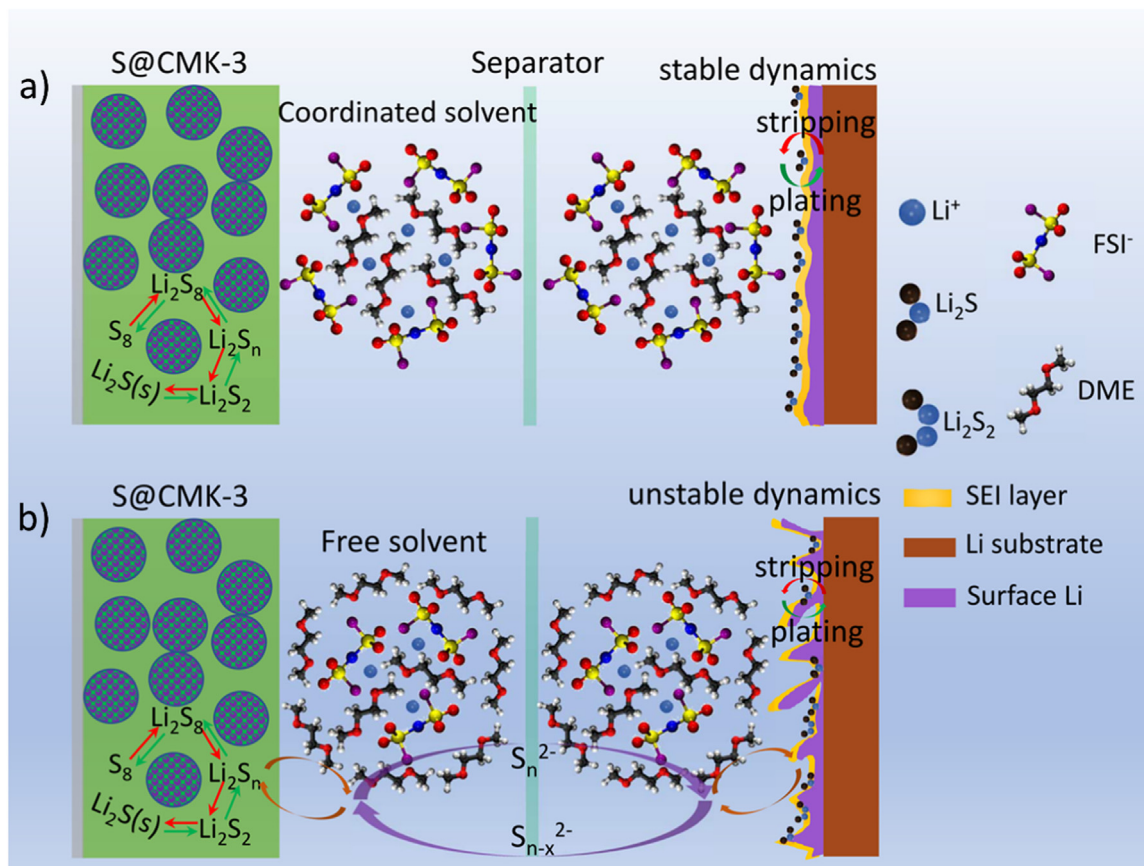
shuttle reaction of polysulfide were also conducted [10]. Recently, novel lithium bis(trifluoromethanesulfonyl)imide (LiTFSI)-based electrolytes with large ionic strength and high viscosity was reported to effectively suppress the dissolution and migration of polysulfide [2a,11]. Specifically, the solvent-salt complex of acetonitrile (ACN)₂:LiTFSI was fabricated as a new class of Li-S battery electrolyte [2a]. However, due to the intrinsic instability between the ACN and Li metal [12], large excess Li metal has to be utilized to achieve a long cycling performance, which largely reduced the energy density of the cell.

Therefore, it remains a severe challenge to identify an electrolyte that can simultaneously overcome the polysulfide shuttle reaction on cathode side and Li dendrite on anode side without sacrificing the capacity utilization of S cathode [13]. Compared with nanostructure engineering strategies, rational design and optimization of electrolytes provide a more economical and viable approach to resolve these issues. In this work, we report such efforts. We formulate a simple electrolyte system using high concentration of LiFSI dissolved in dimethoxyether (DME), without any additives such as LiNO₃ and/or other co-solvents. The rational design leverages the high ionic conductivity and fluorine-rich interphasial chemistry nature of LiFSI as well as low viscosity and electrochemical stability of DME toward Li-metal. This simple electrolyte promotes high reaction dynamics for S cathode even at its saturated concentration. Since the solvent molecules are effectively trapped in the salt solvation sheaths at such extremely high concentration (12 M), the polysulfides dissolution and migration are efficiently inhibited; meanwhile, the irreversible reaction between Li metal and ether solvent is minimized, rendering the major chemical composition of SEI being the reduction products from the anion FSI. The LiF-rich interphase effectively suppresses the formation of lithium dendrites (Scheme 1). Based on the understanding of the mechanisms for suppressing both polysulfide and Li dendrite, a new dilute electrolyte (1 M LiFSI/HFE + DME) is also designed to mimic the mechanism, which achieves

similar electrochemical performances as concentrated electrolytes but with much lower cost.

2. Results and discussion

Compared with the most commonly used lithium bis (trifluoromethane sulfonyl) imide (LiTFSI) salt, lithium bis (fluorosulfonyl) imide (LiFSI) with similar structures possesses excellent properties of extraordinary dissociated ability in common organic solvents, higher ionic conductivity, lower viscosity, and abundant labile fluorine which was expected to lead to a more anion-originated interphase rich in fluorine than LiTFSI does [14]. Its solubility in non-aqueous solvents are also much higher. On the other hand, owing to lone pair electron situating on oxygen, ether-based solvents always serve as strong Lewis bases with major donor numbers, as evidenced by their strong solvation power toward Li⁺. Compared with the cyclic dioxolane molecule (DOL), the linear DME possess a relative higher dielectric constant and lower viscosity; most importantly, its flexibility allows it to form super-molecular chelating structures using both of its oxygens, which leads to much stronger solvation capability for cations [14b,16]. In view of the above properties, an electrolyte of LiFSI/DME system with different concentrations was developed. Undoubtedly the most important parameter for electrolyte is the effective Li⁺ conductivity, which is the portion of current carried by Li⁺, and can be expressed by multiplying the ionic conductivity and the Li⁺ transference number. Although the overall ion conductivity (contributed by both cation and anion) of the electrolyte is reduced at high salt concentration due to the increase in solution viscosity, the Li⁺ transference number, which increases with salt concentration due to the freedom of its diffusion from the solution network [15c], can partially compensate the loss of Li conductivity. The viscosity, ionic conductivity and Li⁺ transference number for LiFSI/DME electrolytes at different concentrations are shown in Fig. S1 and



Scheme 1. Schematic illustration of polysulfide shuttle and lithium dendrite for Li-S batteries in a) concentrated and b) dilute electrolyte, respectively.

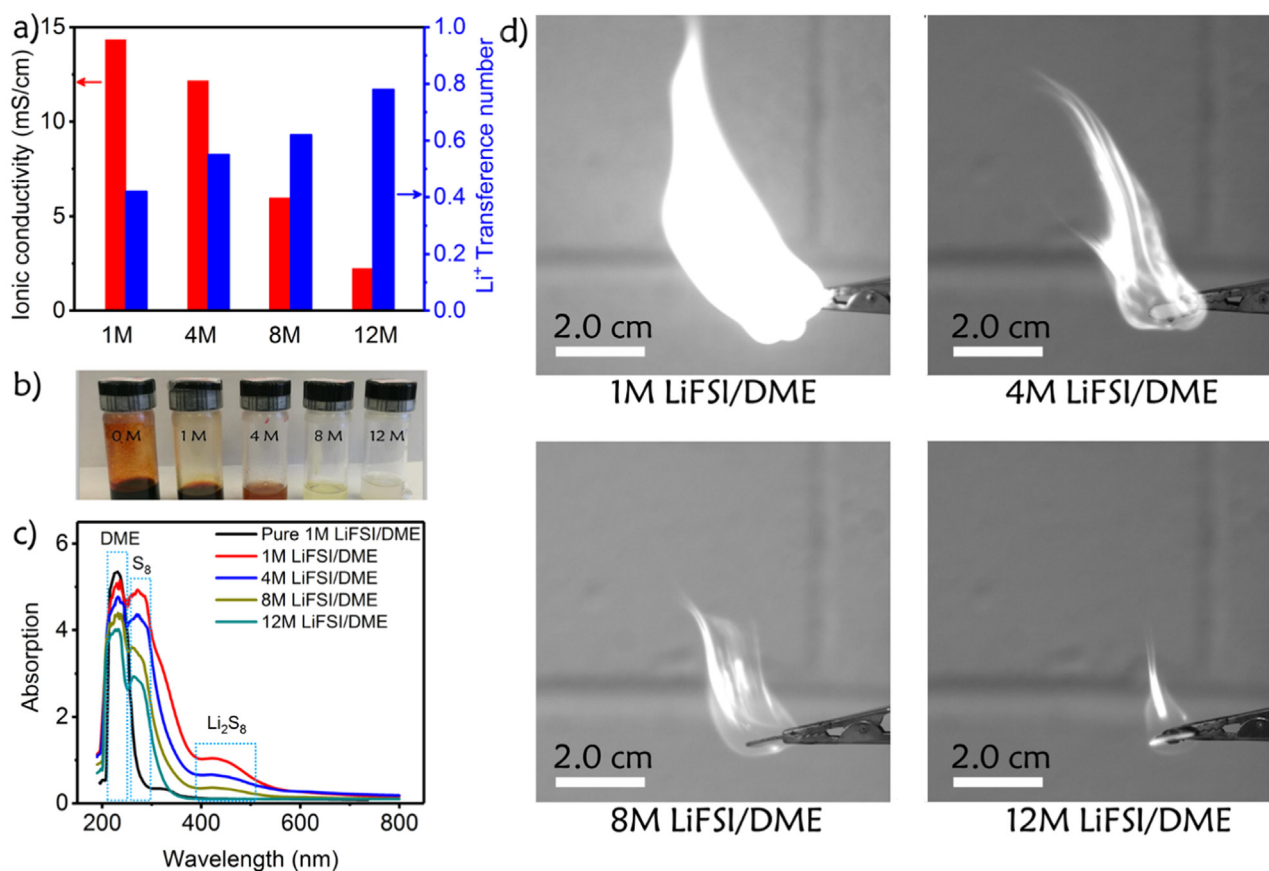


Fig. 1. a) Li⁺ transference number and ionic conductivity versus different salt concentration electrolytes at room temperature. b) and c) are the experiments on lithium polysulfide dissolution: b) typical digital photos of the same amount Li₂S₈ in different electrolytes after standing still for 2 weeks; c) the corresponding UV–vis absorption spectra. d) The ignition experiments of different molarity electrolytes.

Fig. 1a. From 1–8 M the electrolyte viscosity increases with salt concentration, and then level-off after 8 M. The viscosity of high concentration 12 M LiFSI/DME electrolyte (79.6 mPa s) measured at a shear rate of 10 S^{-1} is only twice higher than that of conventional dilute electrolyte (39.9 mPa s for 1 M LiTFSI/DOL + DME) at room temperature (Fig. S1). Although the overall ionic conductivity decreases with salt concentration owing to the formation of abundant Li⁺-solvent clusters, it also reduce the dissolution capability of polysulfide in the electrolyte, thus efficiently suppressing the shuttle reaction. More importantly, the Li⁺ transference number dramatically increases along with the increasing of electrolyte concentration, offsetting the decrease of the ionic conductivity. Thus, these excellent Li⁺ mobility and relatively low viscosity of 12 M LiFSI/DME electrolyte can alleviate the property of sluggish ionic conductivity, providing sufficient Li⁺ transport for electrochemical reactions in Li-S batteries.

The solubility of lithium polysulfide in electrolytes of different salt concentration was evaluated by dissolving Li₂S₈ into these different electrolytes and waited for two weeks to ensure a saturation state. As shown in Fig. 1b, the color of Li₂S₈/electrolyte mixtures gets lighter along with the increasing concentration of these electrolytes, demonstrating that the solubility of polysulfide is significantly reduced at the high salt concentration. The low solubility of polysulfide in highly concentrated electrolyte is also confirmed using UV–vis spectroscopy. As shown in Fig. 1c, the intensity of the wide characteristic peak of Li₂S₈ at nearly 424 nm decreases with salt concentration from 1 M, 4 M, to 8 M, and totally disappears at 12 M. The profile of the Li₂S₈ in 12 M LiFSI/DME electrolyte at nearly 424 nm region totally overlaps with the pure 1 M LiFSI/DME electrolyte, indicating the absence of any Li₂S₈, and suggesting that the dissolution of lithium polysulfide is completely eliminated in this electrolyte. Meanwhile, the characteristic absorption

peaks of DME signal (at about 230 nm) and S₈ signal (~ 270 nm) exist among all electrolytes [16], owing to the same solvent and the raw material for preparing Li₂S₈ polysulfide. The elimination of dissolution and migration of polysulfide in a Li-S battery will remarkably suppress the parasitic shuttle of polysulfides. Ether electrolytes are also known for their high flammability, which often raise concern for their use in large scale batteries. As demonstrated in ignition and combustion tests in air, flammability of the highly concentrated solution was greatly depressed as compared with the dilute electrolytes. Specifically, the flame propagation distance for 1 M LiFSI/DME is ~ 7 cm long and ~ 4 cm wide, while the flame for 12 M LiFSI/DME is only ~ 2 cm × 1 cm (Fig. 1d). Therefore, the higher concentration electrolyte should result in a much safer battery with less flammability in case the cell is vented in presence of sparks (Video S1).

Supplementary material related to this article can be found online at <http://dx.doi.org/10.1016/j.nanoen.2018.05.065>.

Electrochemical performances of Li-S batteries using the S@CMK-3 (68.4 wt% of S) as cathode (Fig. S2) and Li metal as anode were evaluated in different electrolytes. As shown in the cyclic voltammogram (CV) profiles, two reduction peaks and one oxidation peak for sulfur cathode are observed in baseline 1 M LiTFSI/DOL + DME electrolyte (Fig. S3a) [17]. Similar peaks were also observed in 1 M LiFSI/DME electrolyte, as shown in Fig. 2a (top). The two reduction peaks correspond to the reduction of elemental sulfur to high-order polysulfides at around 2.37 V, and further reduction to low-order polysulfides at around 2.02 V [18]. However, there is only one reduction peak observed at about 1.70 V in Fig. 2a (bottom), corresponding to the direct and deep reduction of solid S₈ to solid-state Li₂S [19]. This difference in electrochemical behaviors can be attributed to the changes in competitive solvation of Li⁺ by solvent molecules and FSI⁻ anions. Various

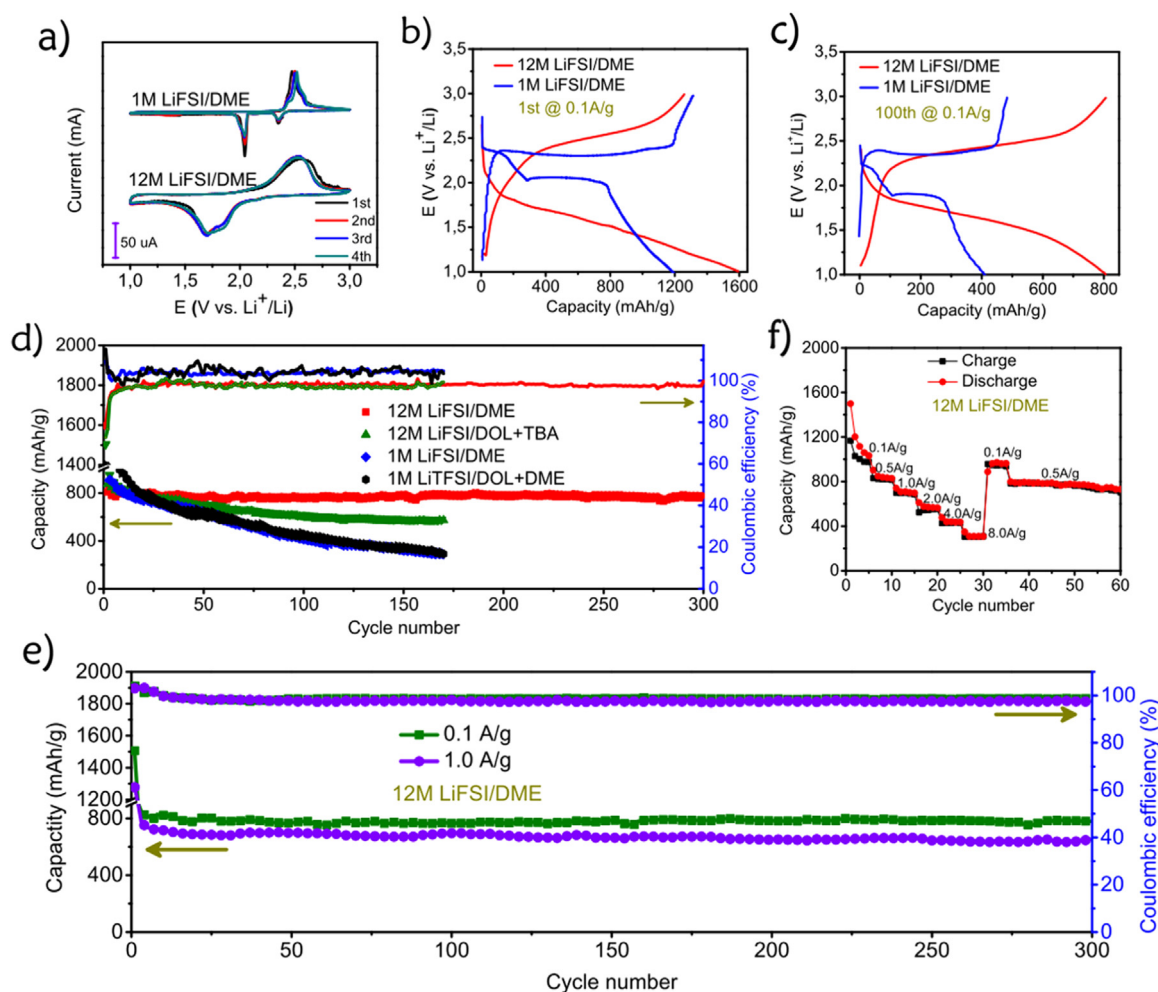


Fig. 2. Electrochemical characteristics of Li-S batteries. a) Cyclic voltammograms in 1 M LiFSI/DME (top) and 12 M LiFSI/DME (bottom) electrolyte at a sweep rate of 0.1 mV/s. Charge-discharge curves at b) 1st and c) 100th cycle in 1 M LiFSI/DME and 12 M LiFSI/DME electrolytes. d) Specific discharge capacity with corresponding CE with different electrolyte. e) Specific discharge capacity with CE over 300 cycles in 12 M LiFSI/DME at the 0.1 A/g and 1 A/g, respectively. f) Rate capability in 12 M LiFSI/DME.

solvation species arise as result from such competition: Li^+ coordinated to solvent-separated ion pair (SSIP), in contact ion pair (CIP), or in aggregate (AGG) that involves multiple cations, anions and solvents. The latter could even extend into dynamic liquid structures in larger scale. The distribution of these solvated species in a solution depends strongly on salt concentration and the structures of solvent and anions. In high concentration electrolytes there is hardly any free solvent molecules, thus a quasi-solid-state reaction mechanism could exist for S chemistry as compared with the solid-liquid-solid reaction well established in dilute electrolyte [20]. This unique reaction mechanism in high concentrated electrolyte promotes direct reduction of S_8 to low-order polysulfide, as evidenced by the absence of Li_2S_8 and Li_2S_6 peak at 2.37 V in CV and the upper plateau at 2.4 V in galvanostatic discharge profiles when measured in 12 M LiFSI/DME (Fig. S3b), which is also consistent with the previously reported electrolyte of 7 M LiTFSI DOL/DME [7]. For 8 M LiFSI/DME, an apparent transitional mechanism from dilute to concentrated electrolyte was observed, with upper reduction peaks weakening from 1st to 4th cycling (Fig. S3c).

Fig. 2b and c showed the galvanostatic discharge/charge voltage profiles at the 1st and 100th cycle of sulfur cathode in 1 M and 12 M LiFSI/DME electrolytes, respectively, at a current density of 100 mA/g. The discharge capacities delivered in the concentrated electrolytes are constantly higher than (or equal to) the charge capacities during these cycles, while the discharge capacities in dilute electrolyte are lower than the charge capacity. This difference reveals that the shuttle

reaction of high-order polysulfide in the dilute electrolyte exist, but entirely disappears in the concentrated electrolyte. Meanwhile, the sulfur in 1 M LiFSI/DME electrolyte showed two distinct reduction plateaus at around 2.3 V and 2.0 V, which can be attributed to the conversion of solid S_8 to soluble high-order polysulfide and then to insoluble low-order $\text{Li}_2\text{S}_2/\text{Li}_2\text{S}$, respectively. However, only one wide voltage plateau at around 1.7 V exists in 12 M LiFSI/DME electrolyte, demonstrating that the high-order polysulfides never formed in the high-concentrated electrolyte, hence without any parasitic shuttle. Furthermore, due to the relatively slow kinetics in solid-state, the overpotential observed in 12 M electrolyte is slightly larger than that in 1 M electrolyte in the first cycle; but the difference gradually vanishes due to the increasing impedances in the dilute electrolytes with cycling. Similar kinetics and stable cycling performance has also been observed in other dilute and concentrated electrolytes based on DOL and TBA solvents (12 M LiFSI/DOL + TBA and 1 M LiTFSI/DOL + DME), as indicated in Figs. S4b and 4c.

Cycling stability and coulombic efficiency of sulfur cathode in these four different electrolytes were evaluated (Fig. 2d and e), where the high-concentrated electrolytes show better cycling stability than diluted electrolytes, with 12 M LiFSI/DME electrolyte being the best, which maintains a reversible discharge capacity of 786 mA h/g at the 300th cycle under the current of 100 mA/g. Importantly, the CE can reach > 99.7% after initial few cycles, which can be attributed to the effective suppression of polysulfide shuttle effect during charging,

while the S cathodes in traditional dilute electrolytes (1 M LiFSI/DME and 1 M LiTFSI/DOL + DME) have a higher CE of 115% and 108% at the initial cycles, respectively, which are caused by the shuttle reaction that transports high order polysulfides to Li surface results in irreversible consumption of the active species and a quick capacity decay. The slightly faster capacity decay (to ~ 576 mA h/g at 175th) for S in 12 M LiFSI/DOL + TBA than that in 12 M LiFSI/DME is due to the easy ring-open polymerization of DOL solvent, which occurs even in the presence of the anti-polymerization stabilizer TBA [21]. When a high current density of 1000 mA/g was applied for S cathode in 12 M LiFSI/DME electrolytes, S still maintains 644 mA h/g for 300th cycles (Fig. 2e). Meanwhile, the sulfur cathode in 12 M LiFSI/DME electrolyte also presents an excellent rate capability, as indicated in Fig. 2f. The discharge capacity of 307 mA h/g is maintained even at a current density of 8.0 A/g after the initial activation at 0.1 A/g and subsequent rate cycles at 0.5, 1.0, 2.0, 4.0, 8.0 A/g. More importantly, when the current density is switched back to its initial value of 0.1 A/g, the initial capacity is also completely recovered, implying the excellent tolerance to the rapid reactions in the highly concentrated electrolyte.

Galvanostatic intermittent titration techniques (GITT) is applied to S cathode to reveal the reaction mechanism in dilute electrolyte (1 M LiTFSI/DME, 1 M LiTFSI/DOL + DME) and concentrated electrolytes (12 M LiTFSI/DME, and 12 M LiFSI/DOL + TBA). As shown in Fig. 3a and b and Fig. S5a and S5b, quasi-equilibrium potential of S cathode in two dilute electrolytes show two discharge plateaus and the overpotential in discharge reaction from Li_2S_2 to Li_2S is much larger than that in discharge process from Li_2S_4 to Li_2S_2 . The initial delithiation of Li_2S experiences a large overpotential, and the overpotential gradually decreases during further delithiation and stabilizes at a small value after forming soluble high-order polysulfide along with long flat potential plateau from shuttle reaction (Fig. 3a), which is in accordance with previously reported results in common 1 M LiTFSI/DOL + DME electrolyte (Fig. S5a) [22]. In contrast, no quasi-equilibrium potential plateaus above 2.3 V was observed in two highly-concentrated electrolytes (12 M LiFSI/DME and 12 M LiFSI/DOL + TBA). Instead, the discharge quasi-equilibrium potential shows only a long slop potential centered at 2.0 V (Fig. 3b). The overpotentials of S cathodes in highly-

concentrated electrolytes maintain the similar values during entire charge/discharge process, which is distinctly different from the dilute electrolyte (Fig. 3a and Fig. S5b). Since no active materials dissolve in the high-concentrated liquid electrolyte, the amount of electrolyte in the high-concentrated electrolyte has been reduced to 3.3 $\mu\text{L}/\text{mA h}$, which is much lower than the electrolyte amount reported Li/S batteries. A stable GITT curve of S cathode during the first five sequential charge/discharge cycles in 12 M LiFSI/DME electrolyte (Fig. 3c) demonstrate that shuttle phenomenon has been thermodynamically inhibited. Therefore a high CE of S cathode with a low electrolyte loading can be realized in a highly-concentrated electrolyte.

The suppression of the shuttle reaction also reduce the self-discharge rate, which has been one of the most severe challenges for the Li-S battery. Fig. 3d and e present the evolution of open-circuit potential for fully charged Li/S cells during the relaxation for 500 h at room temperature using either 12 M LiFSI/DME or 1 M LiFSI/DME electrolyte following 15 activation charge/discharge cycles, respectively. The 15 activation cycles at 0.1 A/g was conducted to ensure the cells are in equilibrium condition. The immediate potential drops upon turning-off the charge current is due to the ohmic, charge-transfer and diffusion polarization. After that, the open-circuit potential of S cathode in 12 M LiFSI/DME electrolyte stabilizes even after nearly 500 h, while a continuous decreasing is observed for 1 M LiFSI/DME electrolyte. The high self-discharge rate in the low concentration electrolyte is caused by the serious shuttle reaction of polysulfides between the cathode and anode [23]. Therefore, the present high-concentrated 12 M LiFSI/DME electrolyte significantly improved the CE of sulfur cathode and completely suppressed the self-charge by eliminating the dissolution of polysulfide into electrolyte and its subsequent migration between the cathode and anode.

The electrochemical behavior of Li metal anode in highly-concentrated electrolyte was also investigated. The cycling stabilities of Li plating/stripping process was investigated in dilute and concentrated electrolytes using Li/Cu coin cells. As demonstrated in Fig. 4a, the Li anode in 12 M LiFSI/DME electrolyte has an initial CE of $\sim 97.8\%$, along with a stable average CE of $\sim 99.2\%$ over 250 cycles. Moreover, such a stable Li depositing/stripping process also can be maintained

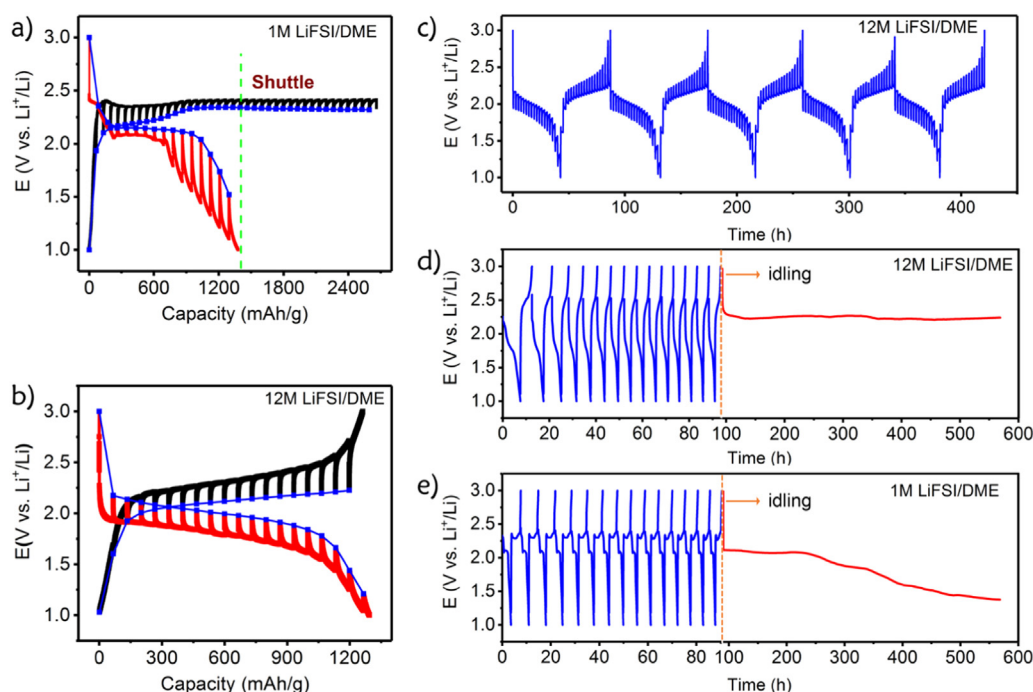


Fig. 3. GITT curves in a) 1 M LiFSI/DME and b) 12 M LiFSI/DME electrolyte. c) 5 successive GITT curve in 12 M LiFSI/DME after 15 activation cycles. Long-term self-discharge characteristics for a Li-S coin cell in d) 12 M LiFSI/DME and e) 1 M LiFSI/DME.

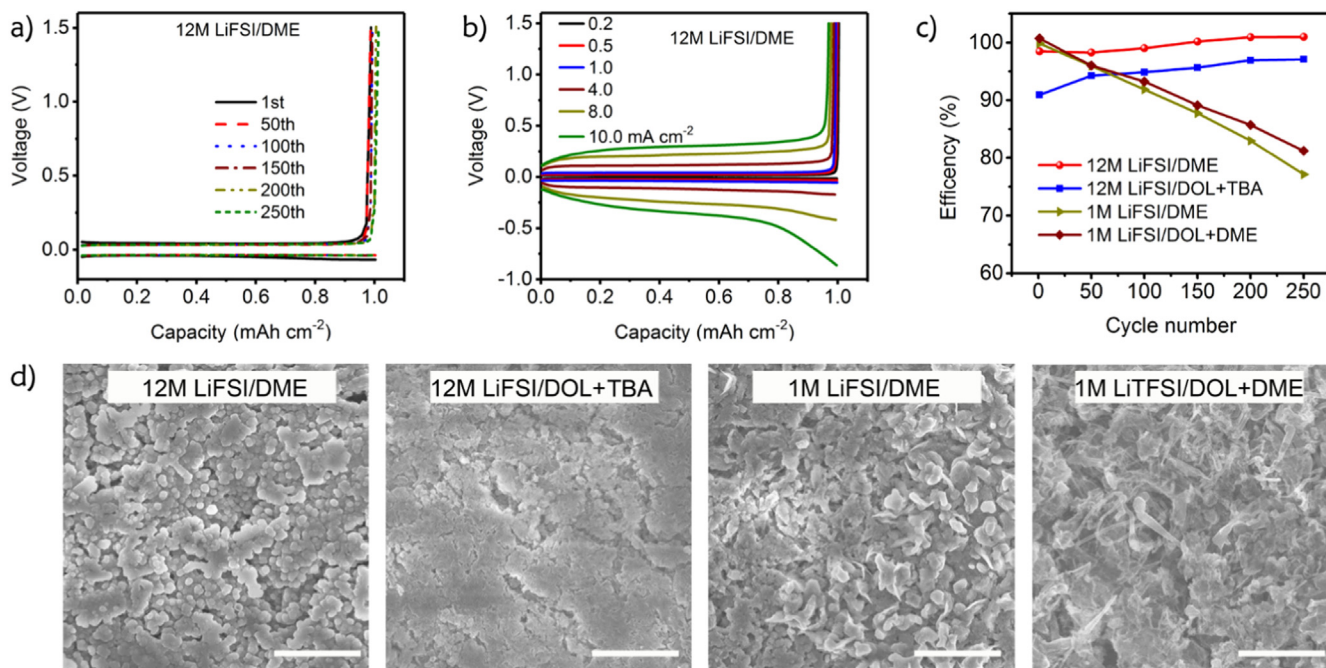


Fig. 4. Voltage profiles of the Li metal plating/stripping on Cu working electrode (Li|Cu cell) in 12 M LiFSI/DME electrolyte a) at 1.0 mA cm^{-2} under different cycles and b) at different current densities. c) A comparison of the Li metal plating/stripping efficiency in different electrolytes over 250 cycles at 1.0 mA cm^{-2} . d) SEM images of Li metal surface in different electrolytes after 100 cycles at a current density of 1.0 mA cm^{-2} (scale bar: $20 \mu\text{m}$).

under different current density, as shown in Fig. 4b. Even at a high current density of 10 mA cm^{-2} , a high CE of $\sim 95\%$ can be reached in the 12 M LiFSI/DME electrolyte. The CE of Li stripping/plating in 12 M LiFSI/DOL + TBA electrolyte is lower (Fig. 4c), which can be attributed to continuous electrolyte decomposition of 12 M LiFSI/DOL + TBA due to the ring-open polymerization of DOL. These results indicated that an excellent reversibility property for Li depositing/stripping can be achieved in the concentration electrolyte, probably owing to high

recovery of Li stripping via controlling the reaction dynamics for Li depositing/stripping process. Although a relatively higher CE can be achieved in the first several cycles for 1 M LiFSI/DME and 1 M LiTFSI/DOL + DME, respectively, the CE of Li anode rapidly decays to 76% and 80% after 250 cycles.

Fig. 4d shows the morphology of Li metal surface after 100 cycles at 1 mA cm^{-2} in different electrolytes. It can be clearly seen that a nodule-like Li layer without dendrite structures was formed on the surface of Li

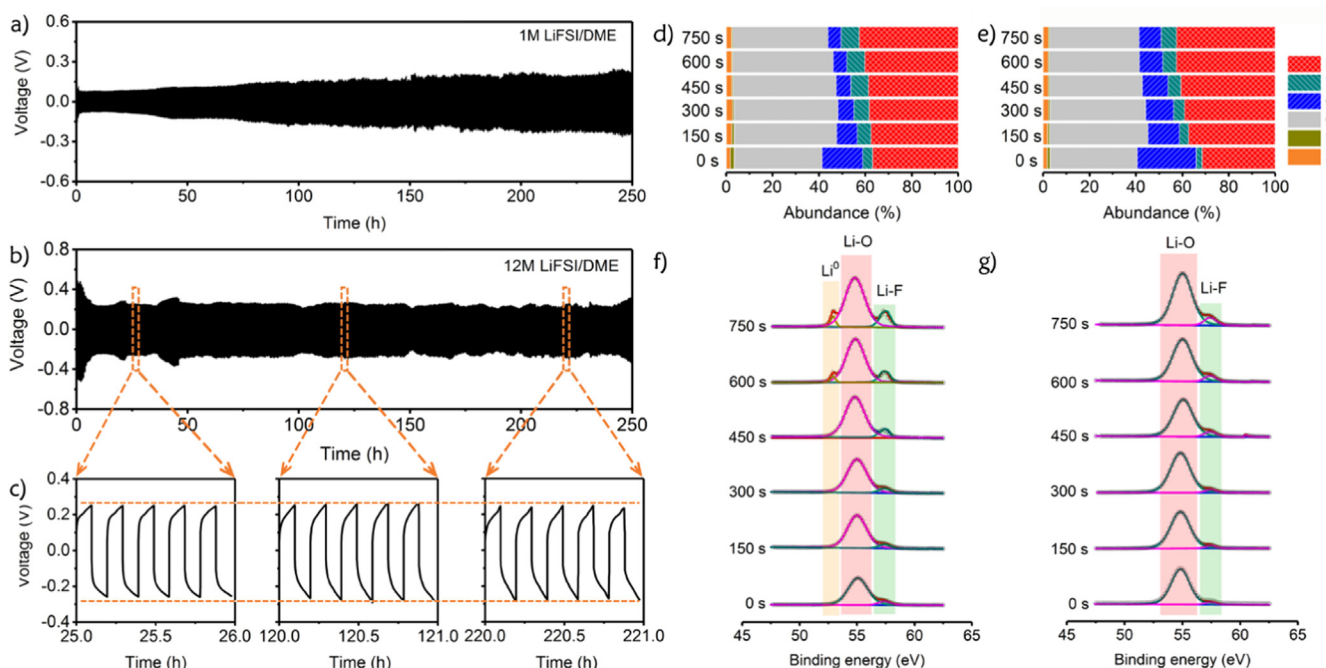


Fig. 5. Voltage profiles during subsequent lithium plating/stripping processes from a Li|Li symmetrical cell at 10 mA cm^{-2} in a) 1 M LiFSI/DME electrolyte, b) 12 M LiFSI/DME electrolyte (The bottom plots of b) are expanded in c). d, e) Element abundance (%) and f, g) high-resolution Li 1s XPS spectra of lithium anode surface after 100 cycles in d, f) 12 M LiFSI/DME and e, g) 1 M LiFSI/DME with different etching time.

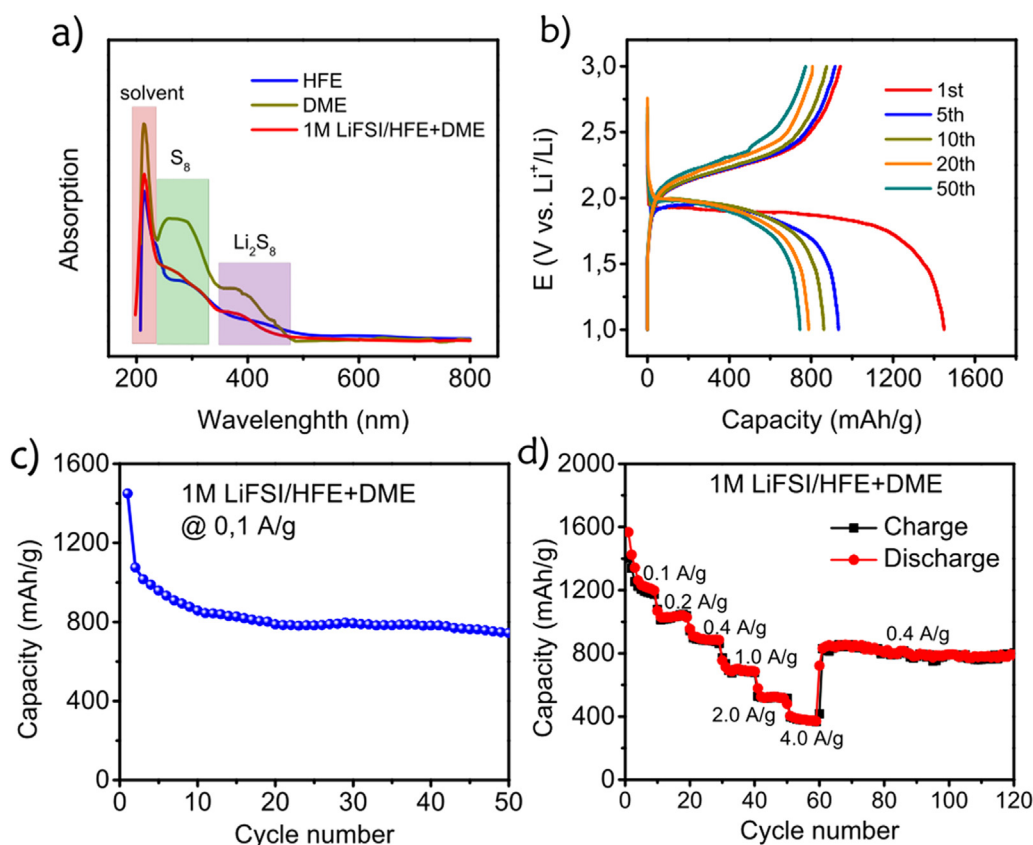


Fig. 6. a) UV-vis spectroscopy of “Li₂S₈-containing DME” solution in electrolyte and different solvents. b) charge/discharge curve, c) its specific discharge capacity of Li-S batteries at 0.1 A/g, and d) rate performance at various current densities in the 1 M LiFSI/HFE + DME electrolyte.

metal in 12 M LiFSI/DME electrolyte. Similar smooth structures on the surface of Li metal can also be observed in 12 M LiFSI/DOL + TBA electrolyte. In contrast, many tiny Li metal dendrite seeds appear on the surface of Li metal in 1 M LiFSI/DME and 1 M LiFSI/DOL + DME electrolytes. These seeds could promote nucleation and continue to grow into needle-like Li dendrites, consuming more electrolyte with its high surface area. This obvious difference in surface structures of Li metal in different electrolytes indicated that the side reactions between Li metal and electrolyte can be effectively minimized by high salt concentration, owing to the strong trapping of solvent molecules in solvation sheaths of Li⁺ [24]. As a result, a high CE of Li metal depositing/stripping in Li|Cu cells can be achieved.

The cycling stabilities of Li metal during depositing/stripping in dilute and concentrated electrolytes were also investigated using a Li|Li symmetrical cell. The voltage profiles of Li/Li cell during Li plating/stripping in 1 M and 12 M LiFSI/DME electrolyte at a constant current of 10 mA cm⁻² is presented in Fig. 5. In 12 M LiFSI/DME electrolyte, overpotential of the lithium plating/stripping maintains stable at 10 mA cm⁻² for 250 h, demonstrating an exceptional cycling reversibility for Li depositing/stripping in this electrolyte (Fig. 5b and c). In comparison, a gradually increase in voltage of Li/Li cell can be observed in 1 M LiFSI/DME electrolyte under the same conditions (Fig. 5a), indicating increasing impedance due to the sustained reactions between electrolyte and Li. Similarly, the overpotential for Li plating/stripping in 12 M LiFSI/DOL + TBA electrolyte is stable (Fig. S7). Because of the high concentration of the ether-based electrolyte with relatively higher viscosity than that of the low molarity electrolyte, the overpotential of Li in the high concentration electrolyte is larger than that of 1 M electrolyte in the beginning. However, the polarization of Li|Li cell in 12 M LiFSI/DME remains stable during charge/discharge cycles; while polarization of Li|Li cell in dilute electrolyte continuously increase due to growth of solid electrolyte interphase

(SEI) [25]. The stable and thin SEI layer on Li in the high concentration ether-based electrolyte stabilize Li deposition/dissolution reaction even at a high current density [7,26].

The nature of SEI film on Li metal in 12 M LiFSI/DME and 1 M LiFSI/DME electrolytes was studied using XPS. After cycling 100 cycles at 0.1 A/g, the composition of SEI on lithium metal foils was characterized using XPS by continuous etching from 0 s to 750 s, as demonstrated in Fig. 5d and g. With the increasing of etching time, the element abundance of C% in SEI obviously decreases, owing to the decomposition of organic solvent in outer-layer of SEI with a relative high potential (away from Li), but the F % increases due to Li salt decomposition at a low potential near to Li (Fig. 5d and e). The composition change is consistent with previous reported results, which the multilayer SEI films mostly consist of outside-organic to inside-inorganic compositions along with depth of the SEI layer [9,27]. Furthermore, a lithium metal signal (Li⁰) appeared in 12 M LiFSI/DME electrolyte after only 600 s etching time, but no signal of Li⁰ peak can be observed in 1 M LiFSI/DME even after 750 s etching. Therefore, a much thicker SEI should have formed in dilute electrolyte than that in concentrated electrolyte. More importantly, the content of Li-F bond in SEI formed in the 12 M electrolyte is much higher than that formed in dilute electrolyte at the same etching time, so a denser LiF-rich SEI was formed in 12 M electrolyte than that in 1 M electrolyte (Fig. 5f and g). The electronic insulating LiF-rich SEI layer is formed in 12 M concentrated electrolyte reduce the SEI thickness [28b,29], and the high interface energy of LiF with Li metal suppresses the Li dendrite growth in vertical direction.

Based on these analysis, we can conclude that the superior electrochemical performance of the Li-S batteries in highly-concentrated electrolyte are due to following two reasons: 1) the ultra-high concentrated electrolyte without free solvent restricted the possible dissolution of the polysulfides; 2) the LiF-rich SEI layer, formed mainly

from the reduction of salt anion on the Li anode, dramatically increasing the Li metal cycling stability and the CE. The combination of these two features significantly enhance the cycling stability of Li/S cell without any shuttle reaction.

In the electrolyte, the cost of lithium salt is the highest portion. Even through the price of the LiFSI reduced by 90% in the last two years because more chemical companies began to manufacture the LiFSI salt (Fig. S8), the price of the high concentrated 12 M LiFSI electrolyte is still higher than that of the common 1 M electrolytes. Therefore, a more realistic approach is to reduce the salt concentration to the normal level (1 M) in the electrolyte. Based on the understanding of the electrochemical mechanism of the highly concentrated electrolyte, we developed diluted electrolyte (1 M LiFSI DME/HFE) electrolyte, which shows similar properties compared with the highly concentrated electrolyte. HFE that does not dissolve the LiFSI salt was added into high concentrated electrolyte to form an apparent dilute 1 M LiFSI in HFE/DME ($v/v = 96:4$) but localized concentrated electrolyte. Since HFE solvent cannot dissolve the salt, this diluent actually compresses the solvent DME and the salt dissolves into a tiny local region, forming a localized super-concentration. The dissolution of lithium polysulfide species in this electrolyte was analyzed by UV-vis spectroscopy, as shown in Fig. 6a. Because there is a low donor ability and permittivity for HFE, the HFE rarely participates in the solvation, resulting in a minimized solubility of polysulfide. When small amount of Li_2S_8 was added into the HFE, only a solvent peak can be detected at the wavelength of about 230 nm, without any existence of S_8 and Li_2S_8 peaks (the very slight S_8 and Li_2S_8 peaks came from the DME solvent in prepared Li_2S_8 solution). For comparison, when the same amount of Li_2S_8 added into DME solvent, the DME, S_8 and Li_2S_8 peaks can be clearly observed because of the high solubility of polysulfide in DME. In this localized-concentrated electrolyte, all the LiFSI salts are confined to the regimes with the DME, which results in minimum polysulfide dissolution in the bulk electrolyte consisting of non-solvent. The electrochemical performance of charge/discharge curve with its specific discharge capacity in this dilute (local concentrated) electrolyte were demonstrated in Fig. 6b and c. The discharge curves exhibit only a single voltage plateau near 2.0 V during cycling without the 2.3 V reduction plateau corresponding to the transformation from S_8 to high-order polysulfide, similar to S chemistry in 12 M LiFSI/DME electrolyte. This result can be attributed to the direct and deep solid-to-solid (solid S_8 to insoluble Li_2S) phase transition in both pseudo dilute and concentration electrolyte [19]. Especially, the supersaturation of polysulfur have been achieved in both concentrated electrolyte without free soluble DME solvent and in localized concentrated electrolyte with non-solvent HFE, both leading to the insolubility of high-order polysulfides and direct reduction. As a result, S cathode in this 1 M LiFSI/HFE + DME pseudo dilute electrolyte also exhibits excellent cycle stability. The first discharge in the 1 M pseudo concentration displays a much high capacity of 1449 mA h/g (for sulfur) with high sulfur cathode utilization, and maintains a reversible capacity of 774 mA h/g at 50th cycles. It can be observed that there is a fairly large irreversible capacity in the 1st cycle in the HFE/DME electrolyte. This phenomenon is totally different from the most common used electrolyte of 1 M LiTFSI DME/DOL. The 1 M LiTFSI DME/DOL electrolyte is relatively stable in the operating voltage range (1–3 V) for the Li-S cells, therefore the discharge capacity due to the formation of the SEI is rather limited [29]. Instead, the shuttle reactions may even result in a larger charge capacity than the initial discharge capacity [29]. However, for the concentrated 12 M LiFSI DME electrolyte or in the 1 M LiFSI/HFE + DME local high-concentrated electrolytes, almost all of the DME are bonded with Li^+ and FSI⁻. These concentrated FSI⁻ anions can easily be reduced at relatively high voltage of ~ 1.5 V [30]. The cleavage of the S–F bond in FSI⁻ anion can lead to a thermodynamically stable LiF, which coated on the surface of the S@CMK-3 cathode [30]. The in situ formed SEI layer on the S@CMK-3 due to the reduction of the FSI⁻ anions provides some irreversible capacity in the first cycles in the concentrated electrolyte or in the 1 M

LiFSI/HFE + DME. Meanwhile the polysulfide shuttle reactions are totally suppressed. Therefore, only the S that has good contact with the CMK-3 can provide the capacity. In the lithiation process, the S will possess a high volume change of 80% [31]. In the first several cycles, some S will break down from the CMK-3 matrix, and thereby results in the capacity decay. These factors altogether result in the “fairly large” irreversible capacities in the first several cycles (especially for the initial cycle) in the 1 M LiFSI/HFE + DME electrolyte.

Fig. 6d demonstrates the rate performance of Li-S battery in 1 M LiFSI/HFE + DME electrolyte. A discharge capacity of 1198 mA h/g is obtained with current density of 0.1 A/g; meanwhile, a high discharge capacity of 1028, 864, 689, 516, 371 mA h/g is achieved at 0.2 A/g, 0.4 A/g, 1.0 A/g, 2.0 A/g, 4.0 A/g, respectively. Moreover, as the current density changes back to 0.4 A/g, the capacity can return to 831 mA h, indicating highly reversibility of rapid reaction mechanism in the 1 M LiFSI/HFE + DME electrolyte.

3. Conclusion

In conclusion, we developed a stable and safe highly concentrated electrolyte for efficient Li-S battery. The shuttle effect of lithium polysulfide and the growth of lithium dendrites in Li-S battery were simultaneously suppressed by the formation of robust LiF-rich SEI with high interface energy and controllable Li plating/stripping kinetics, which yield the highest Coulombic efficiencies for the S cathode (99.7%) and the Li anode (99.2%). Such unique electrochemical properties for high concentrated electrolytes further inspired us to design a more practical pseudo-high-concentration electrolyte by using of a “non-solvent” to reduce the cost of the salt. Similar electrochemical performances were achieved when compared with the high concentrated electrolyte. These discoveries provide valuable guidance to the accelerate the commercial applications of the next generation high-performance Li-S batteries.

4. Experimental section

4.1. Materials and synthesis

The electrolytes are prepared as follows: lithium bis (fluoro sulphonyl) imide ($\text{LiN}(\text{SO}_2\text{F})_2$, LiFSI) and lithium bis (trifluoromethane sulphonyl) imide ($\text{LiN}(\text{SO}_2\text{CF}_3)_2$, LiTFSI) purchased from TCI were used as received. 1,2-dimethoxyethane (DME), 1,3-dioxolane (DOL), Tributylamine (TBA) were obtained from Sigma-Aldrich. 1,1,2,2-tetrafluoroethyl 2,2,3,3-tetrafluoropropyl ether (HFE) were purchase from TCI. The electrolytes were prepared by dissolving a certain amount of salt into the corresponding solvent. Specifically, the LiFSI salt was added into DME solvent to receive 12 M LiFSI/DME electrolyte. Here, “M” stands for molar concentration, i.e., mole of salt dissolved in a liter of solvent (not the electrolyte solution). In addition, different concentrated LiFSI/DME electrolytes (1 M, 4 M, and 8 M) can also be obtained with similar method. Another contrast electrolyte of 12 M LiFSI/DOL + TBA can be prepared with 12 M LiFSI in DOL solvent with 1 wt % of TBA (TBA is used to suppress the ring-open reactions of DOL) [21]. The reference electrolyte (1 M LiTFSI/DOL + DME) was composed of 1 M LiTFSI in a mixed solvent of DOL/DME ($v/v = 1:1$). Another pseudo dilute electrolyte (1 M LiFSI/HFE + DME) was also prepared by dissolving 1 M LiFSI salt in a mixed solvent of HFE/DME ($v/v = 96:4$). Because HFE solvent cannot dissolve the salt, the pseudo dilute electrolyte is actually another concentration electrolyte. The carbon/sulfur composite (S@CMK-3) was prepared by a melting sulfur diffusion method. In detail, a certain amount of CMK-3 and sulfur were uniformly grounded together, sealed in a glass tube under vacuum, and then heated at 155 °C for 15 h.

4.2. Structural characterization

X-ray diffraction analysis (XRD) patterns were recorded by Bruker Smart 1000 (Bruker AXS Inc., USA) using Cu K α line radiation source. Scanning electron microscopy (SEM) images were observed on a Hitachi SU-70 field emission scanning electron microscope (S4800, HITACHI, Japan). Thermogravimetric Analysis-Differential Scanning Calorimetry (TG-DSC) (TA Instruments, USA) was carried out under Argon gas with a heating rate of 5 °C/min. X-ray photoelectron spectroscopy (XPS) was achieved on a monochromatized ESCALAB 250 X-ray with Al K α source radiation with an Ar⁺ ion sputtering gun. Sample viscosity was measured using an AR2000 stress-controlled rheometer (TA Instruments), running at 25 °C on a cone-and-plate geometry (20 mm diameter, 2° cone angle). A solvent trap was used to minimize evaporation of the solvent during measurements. The experiments were conducted under steady shear, and the apparent viscosity was measured as a function of the shear rate. The viscosity values reported here correspond to a shear rate of 10 s⁻¹. The preparation of lithium polysulfide dissolution was carried out as following: a mole ratio of Li₂S and S (1:7) were mixed uniformly in an Argon-filled glovebox and then added into the DME solvent, coming into being with the “Li₂S₈-containing DME” solution. The electrolyte ignition and combustion experiment was observed and recorded by high-speed digital camera with a Vision Research Phantom v 12.1 digital camera; and the frame rate of 1000 frames per second with a resolution of 640 × 480 pixel. A small piece of glass fiber membrane was soaked with ~ 0.5 mL electrolyte solution and fixed by an alligator clip, followed by immediate ignition with a butane lighter.

4.3. Electrochemical measurement

The working electrode preparation: S@CMK-3 composite, conductive carbon, polyvinylidene difluoride (PVDF) with a weight ratio of 8:1:1 were mixed in certain amount of N-methylpyrrolidinone (NMP) solvent to form homogeneous slurry by stirring for 4 h. The slurry was coated onto a thin Al foil and dried at 65 °C for 14 h in vacuum. The coin cells (CR2032) were assembled with the prepared working electrode, pure lithium metal foil as counter electrode, a sheet of polypropylene microporous (PP Celgard) film as separator in an argon-filled glove box. The galvanostatic charge/discharge tests were performed with Arbin Battery test instrument (BT2000, Arbin Instruments, USA) at a voltage range of 1.0–3.0 V versus Li/Li⁺ at room temperature (23 ± 0.5 °C). The galvanostatic intermittent titrations (GITT) were also tested on the Arbin station by alternating the current density of 0.1 A/g for 20 min along with open circuit voltage periods of 120 min after 15 cycle's charge/discharge activation cycles. The Li anode CE in various electrolytes was tested using Li|Cu coin cells (CR2032) which were assembled in the argon-filled glove box, employing Li foil with a diameter of 14 mm as both the counter and reference electrode, Cu foil with a same diameter to Li foil as the substrate for Li metal stripping/deposition, and polypropylene microporous film (PP Celgard) as separator. Different current densities for Li metal plating/stripping process was set by using Arbin Battery test instrument (BT2000, Arbin Instruments, USA) at room temperature. For each current density, the deposition capacity for Li metal on Cu foil is 1 mA h cm⁻², with a stripping voltage up to 1.5 V versus Li/Li⁺. The same Arbin stations were used to conduct the electrolyte cycling efficiency tests of and Li|Li coin cells (CR2032), with the similar experimental procedure of Li|Cu cells except the Li foil replacement of Cu foil. Cyclic voltammetry (CV) measurements were performed on a CHI660D electrochemical workstation with a scan rate of 0.1 mV/s (CH Instrument, Shanghai, China).

Acknowledgements

J. Z. and X. F. contributed equally to this work. The authors thank the support from the Nanostructures for Electrical Energy Storage

(NEES), an Energy Frontier Research Center funded by the U.S. Department of Energy, Office of Science, Basic Energy Sciences under Award number DESC0001160. The authors gratefully acknowledge the support of the Maryland NanoCenter and its AIM Lab. J.W acknowledges Heilongjiang Province Natural Science Foundation (key project) (ZD2016-001) and Jiamusi University Interdisciplinary Project (12J201502)

Conflict of interest

The authors declare no competing financial interest.

Appendix A. Supplementary material

Supplementary data associated with this article can be found in the online version at <http://dx.doi.org/10.1016/j.nanoen.2018.05.065>.

References

- [1] a) J. Qian, W.A. Henderson, W. Xu, P. Bhattacharya, M. Engelhard, O. Borodin, J.G. Zhang, *Nat. Commun.* 6 (2015) 6362; b) N.S. Choi, Z. Chen, S.A. Freunberger, X. Ji, Y.K. Sun, K. Amine, G. Yushin, L.F. Nazar, J. Cho, P.G. Bruce, *Angew. Chem. Int. Ed.* 51 (2012) 9994–10024; c) L. Suo, Y.S. Hu, H. Li, M. Armand, L. Chen, *Nat. Commun.* 4 (2013) 1481.
- [2] a) M. Cuisinier, P.E. Cabelguen, B.D. Adams, A. Garsuch, M. Balasubramanian, L.F. Nazar, *Energy Environ. Sci.* 7 (2014) 2697–2705; b) Q. Pang, X. Liang, C. Kwok, L.F. Nazar, *J. Electrochem. Soc.* 162(1015) A2567–A2576.
- [3] a) G. Zheng, S.W. Lee, Z. Liang, H.W. Lee, K. Yan, H. Yao, H. Wang, W. Li, S. Chu, Y. Cui, *Nat. Nanotechnol.* 9 (2014) 618–623; b) K. Yan, H.W. Lee, T. Gao, G. Zheng, H. Yao, H. Wang, Z. Lu, Y. Zhou, Z. Liang, Z. Liu, *Nano Lett.* 14 (2014) 6016–6022.
- [4] N.W. Li, Y.X. Yin, C.P. Yang, Y.G. Guo, *Adv. Mater.* 28 (2016) 1853–1858.
- [5] W. Xu, J. Wang, F. Ding, X. Chen, E. Nasybulin, Y. Zhang, J.G. Zhang, *Energy Environ. Sci.* 7 (2014) 513–6517.
- [6] W.A. Henderson, F. McKenna, M.A. Khan, N.R. Brooks, V.G. Young, R. Frech, *Chem. Mater.* 17 (2015) 2284–2289.
- [7] L. Suo, Y.S. Hu, H. Li, M. Armand, L. Chen, *Nat. Commun.* 4 (2013) 1481.
- [8] M.S. Park, S.B. Ma, D.J. Lee, D. Im, S.G. Doo, O. Yamamoto, *Sci. Rep.* 4 (2014) 3815.
- [9] D. Aurbach, E. Granot, *Electrochim. Acta* 42 (1997) 697–718.
- [10] a) A. Shyamsunder, W. Beichel, P. Klose, Q. Pang, H. Scherer, A. Hoffmann, G.K. Murphy, I. Krossing, L.F. Nazar, *Angew. Chem. Int. Ed. Engl.* 56 (2017) 6192–6197; b) N. Xu, T. Qian, X. Liu, J. Liu, Y. Chen, C. Yan, *Nano Lett.* 17 (2017) 538–543; c) J. Scheers, S. Fantini, P. Johansson, *J. Power Sour.* 255 (2014) 204–218.
- [11] E.S. Shin, K. Kim, S.H. Oh, W.I. Cho, *Chem. Commun.* 49 (2013) 2004–2006.
- [12] Y. Yamada, K. Furukawa, K. Sodeyama, K. Kikuchi, M. Yaegashi, Y. Tateyama, A. Yamada, *J. Am. Chem. Soc.* 136 (2014) 5039–5046.
- [13] Z.W. Seh, Y. Sun, Q. Zhang, Y. Cui, *Chem. Soc. Rev.* 45 (2016) 5605–5634.
- [14] a) J. Hu, G. Long, S. Liu, G. Li, X. Gao, *Chem. Commun.* 50 (2014) 14647–14650; b) K. Xu, *Chem. Rev.* 104 (2004) 4303–4418.
- [15] a) D.R. Chang, S.H. Lee, S.W. Kim, H.T. Kim, *J. Power Sour.* 112 (2002) 452–460; b) K. Xu, *Chem. Rev.* 114 (2014) 11503–11618; c) O. Borodin, L. Suo, M. Gobet, X. Ren, F. Wang, A. Faraone, J. Peng, M. Olguin, M. Schroeder, M.S. Ding, *ACS Nano* 11 (2017) 10462–10471.
- [16] a) A. Kawase, S. Shirai, Y. Yamoto, R. Arakawa, T. Takata, *Phys. Chem. Chem. Phys.* 16 (2014) 9344–9350; b) M.U. Patel, R. Demir-Cakan, M. Morcrette, J.M. Tarascon, M. Gaberscek, R. Dominko, *ChemSusChem* 6 (2013) 1177–1181.
- [17] R. Elazari, G. Salitra, A. Garsuch, A. Panchenko, D. Aurbach, *Adv. Mater.* 23 (2011) 5641–5644.
- [18] C. Barchasz, F. Molton, C. Duboc, J.C. Leprêtre, S. Patoux, F. Alloin, *Anal. Chem.* 84 (2012) 3973–3980.
- [19] S.S. Zhang, *Front. Energy Res.* 1 (2013) 10.
- [20] D.W. Wang, Q. Zeng, G. Zhou, L. Yin, F. Li, H.M. Cheng, I.R. Gentle, G.Q.M. Lu, *J. Mater. Chem. A* 1 (2013) 9382–9394.
- [21] D. Aurbach, E. Zinigrad, H. Teller, P. Dan, *J. Electrochem. Soc.* 147 (2000) 1274–1279.
- [22] Y. Lu, X. Li, J. Liang, L. Hu, Y. Zhu, Y. Qian, *Nanoscale* 8 (2016) 17616–17622.
- [23] F. Jeschull, D. Brandell, K. Edström, M.J. Lacey, *Chem. Commun.* 51 (2015) 17100–17103.
- [24] X.B. Cheng, R. Zhang, C.Z. Zhao, F. Wei, J.G. Zhang, Q. Zhang, *Adv. Sci.* 3 (2016) 1500213.
- [25] G. Bieker, M. Winter, P. Bieker, *Phys. Chem. Chem. Phys.* 17 (2015) 8670–8679.
- [26] K.K. Fu, Y. Gong, B. Liu, Y. Zhu, S. Xu, Y. Yao, W. Luo, C. Wang, S.D. Lacey, *J. Dai, Sci. Adv.* 3 (2017) e1601659.
- [27] a) D. Aurbach, I. Weissman, A. Schechter, H. Cohen, *Langmuir* 12 (1996) 3991–4007; b) D. Aurbach, *J. Power Sour.* 89 (2000) 206–218.

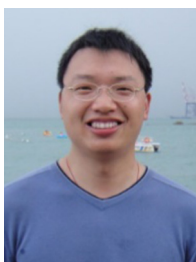
- [28] Q. Zhang, J. Pan, P. Lu, Z. Liu, M.W. Verbrugge, B.W. Sheldon, Y.T. Cheng, Y. Qi, X. Xiao, *Nano Lett.* 16 (2016) 2011–2016.
- [29] S.S. Zhang, *J. Power Sour.* 231 (2013) 153–162.
- [30] a) X. Fan, L. Chen, X. Ji, T. Deng, S. Hou, J. Chen, J. Zheng, F. Wang, J. Jiang, K. Xu, C. Wang, *Chem* 4 (2018) 174–185;
b) H. Kim, F. Wu, J.T. Lee, N. Nitta, H.T. Lin, M. Oschatz, W.I. Cho, S. Kaskel, O. Borodin, G. Yushin, *Adv. Energy Mater.* 5 (2015) 1401972.
- [31] X. Liang, C. Hart, Q. Pang, A. Garsuch, T. Weiss, L.F. Nazar, *Nat. Commun.* 6 (2015) 5682.



Jing Zheng started her M.S. and Ph.D. degree in Nanjing University of Aeronautics and Astronautics, China. She is currently a joint Ph.D. candidate at the Department of Chemical & Biomolecular Engineering, University of Maryland-College Park. Her research interests focus on novel materials and electrolytes for electrochemical energy storage and conversion, including lithium-ion, potassium-ion batteries and lithium-sulfur batteries.



Dr. Xiulin Fan received his bachelor's degree and Ph.D. degree both in Materials Science and Engineering from Zhejiang University. He is currently an assistant research scientist at University of Maryland-College Park. His research interests are novel materials, novel electrolytes and their application in energy storage and conversion devices including lithium-ion batteries, sodium-ion batteries and hydrogen storage.



Prof. Guangbin Ji is a Professor in Materials Science in College of Materials Science and Technology, Nanjing University of Aeronautics and Astronautics (NUAA). He received his Ph.D. Degree (2004) in Laboratory of Solid State Microstructures, Nanjing University, then joined NUAA in 2004. In 2008, he worked in nanomaterials at Department of Physics, Université de Reims, France under a Visiting Professorships program. His current interests are the study on novel materials for magnetism and energy storage and conversion.



Dr. Haiyang Wang received his B.S. degree in Safety Engineering and Ph.D. degree in Engineering Mechanics from Nanjing University of Science and Technology. He is currently a post-doctoral associate in Dr. Michael R. Zachariah's group at University of Maryland-College Park. His research interests are preparation, ignition and combustion characterization of energetic materials. He has more than 20 peer-reviewed journal publications.



Singyuk Hou is a Ph.D. student in the Department of Chemical and Biomolecular Engineering, University of Maryland-College Park. She received her B.S degree (2012) in Chemistry from Wuhan University, China and M.S. degree (2015) in Chemistry from University of Massachusetts, Amherst. Her research interests include magnesium and lithium metal battery and transport kinetic in electrode.



Kerry C. DeMella received her B.S. from Virginia Tech and her M.S. from University of Maryland in Chemistry. She is currently a Ph.D. candidate at the University of Maryland-College Park. Her research interests include polymer capsule design, hydrogel and polymer synthesis, and applications in soft materials.



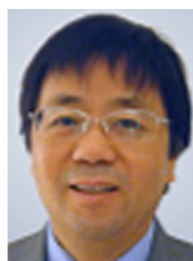
Dr. Srinivasa R. Raghavan is a Full Professor at the University of Maryland, College Park (UMCP). He received his Ph.D. from North Carolina State University, where he studied composite electrolytes for lithium-ion batteries. His research at UMCP has resulted in more than 150 publications and 20 U.S. patents. He was recently designated a “Distinguished Scholar-Teacher” by UMCP, and he has been a three-time nominee for the UMCP “Invention of the Year”. He is the scientific co-founder of several startup companies based on technologies invented in his laboratory.



Dr. Jing Wang is a Professor in College of Material Science and Engineering, Jiamusi University in China. She received her Ph.D. degree from Harbin Institute of Technology. She worked as visiting scholar in the laboratory of Prof. Chunsheng Wang at Maryland University-College Park in 2012–2013. Her currently research interest focuses on nanostructural materials for storage and conversion.



Dr. Kang Xu received his B.S. degree in Chemistry from Southwest Normal University, in 1985 and M.S. in Polymer Chemistry from Lanzhou Institute of Chemical Physics, Academy of Sciences, in 1988. He received his Ph.D. degree in Chemistry in 1996 at Arizona State University. He was employed by the U.S. Army Research Laboratory (ARL) in 2002. He is an ARL Fellow and Team Leader. His research interests concern electrolyte development for electrochemical energy storage applications, which include lithium/sodium ion batteries and electrochemical capacitors.



Prof. Chunsheng Wang is a full professor at University of Maryland College Park (UMCP). He was educated in materials science and trained in electrochemistry and got his Ph.D. degree from Zhejiang University. He has more than 150 peer-reviewed journal publications and more than 25 years of experience in battery research. His Li ion battery research has been highlighted in EFRC news by DoE in 2012, and by Chemical & Engineering News in 2013. He is a recipient of the University of Maryland Outstanding Junior Researcher Award.

Supporting Information

Manipulating electrolyte and solid electrolyte interphase to enable safe and efficient Li-S batteries

Jing Zheng^{a,b†}, Xiulin Fan^{a†}, Guangbin Ji^b, Haiyang Wang^a, Singyuk Hou^a, Kerry C. DeMella^c,
Srinivasa R. Raghavan^a, Jing Wang^d, Kang Xu^e, Chunsheng Wang^{a*}

^a *Department of Chemical and Biomolecular Engineering University of Maryland, College Park, MD 20742, USA*

^b *College of Materials Science and Technology, Nanjing University of Aeronautics and Astronautics, Nanjing 210016, P. R. China*

^c *Department of Chemistry and Biochemistry, University of Maryland, College Park, MD 20742, USA*

^d *School of Materials Science and Engineering, Jiamusi University, Jiamusi 154007, P. R. China*

^e *Electrochemistry Branch, Power and Energy Division Sensor and Electron Devices Directorate, U.S. Army Research Laboratory, Adelphi, MD 20783, USA*

* *Corresponding author, Prof. Chunsheng Wang, Tel.: 301.405.0352, Fax: 301.314.9216, E-mail: cswang@umd.edu*

J.Z. and X.F. contributed equally to this work.

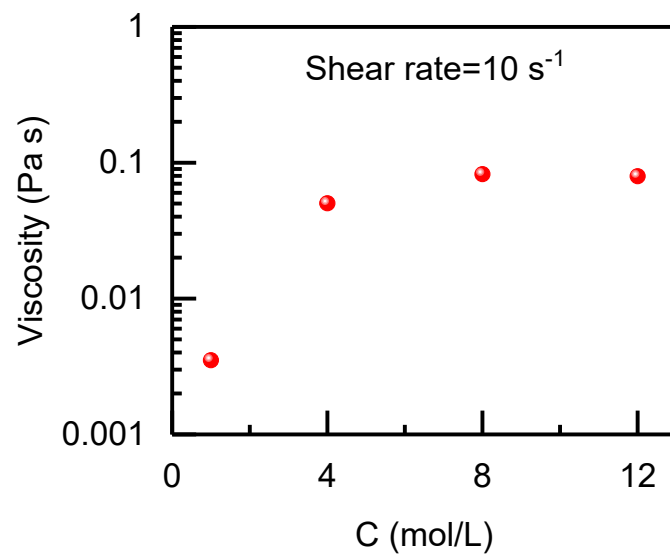


Figure S1. Viscosity for different concentration electrolytes at room temperature with shear rate of 10 s^{-1} .

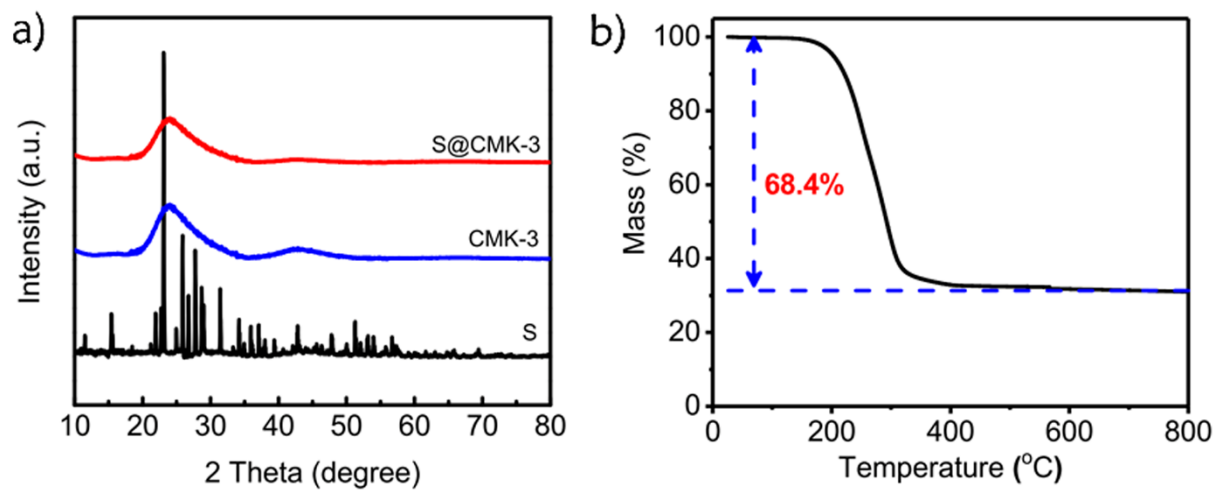


Figure S2. a) XRD patterns of S, CMK-3, and S@CMK-3 composite. b) TG curve of S@CMK-3 composite in Ar with a rate of 5 °C/min.

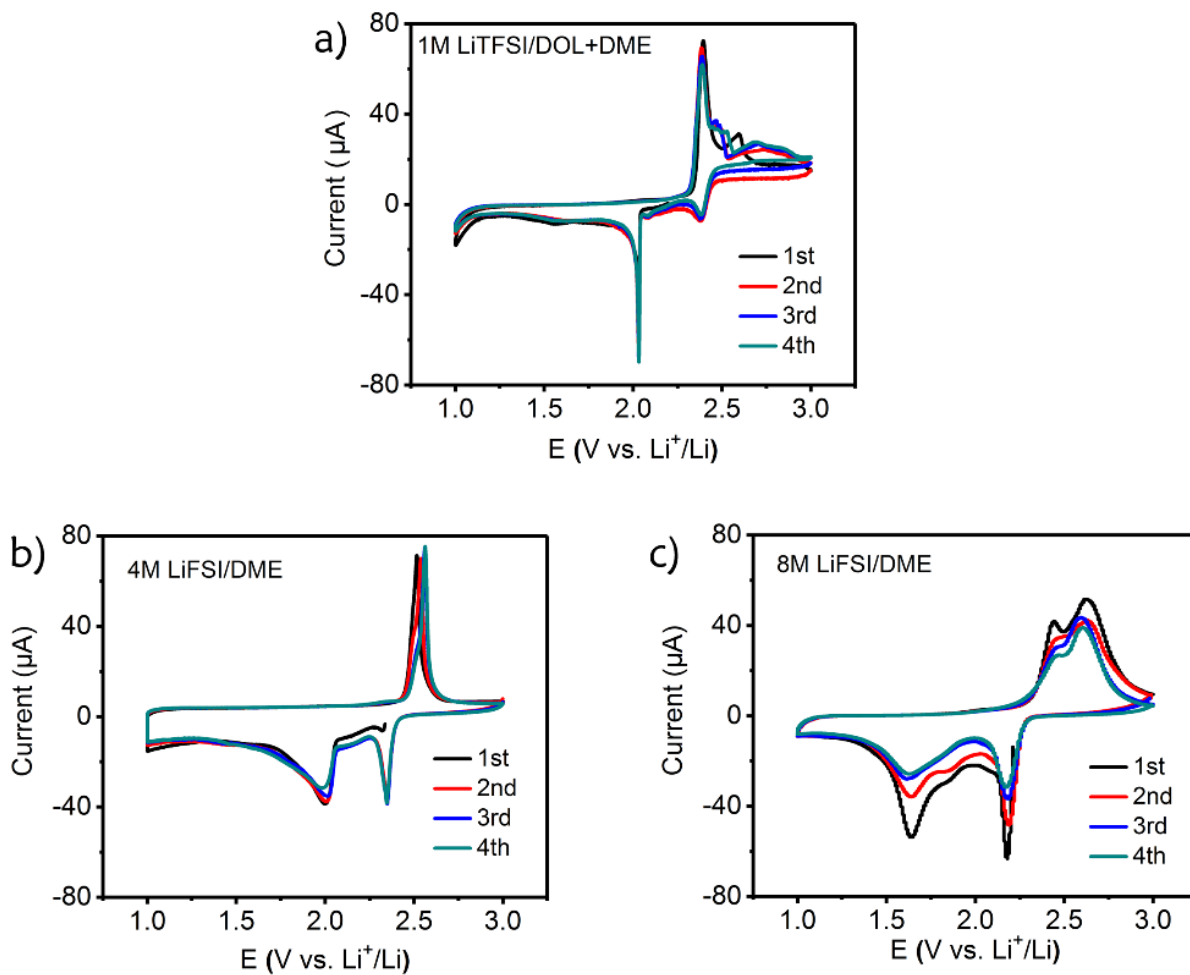


Figure S3. Cyclic voltammograms for a Li-S battery in a) 1M LiTFSI/DOL+DME, b) 4M LiFSI/DME, and c) 8M LiFSI/DME electrolyte with a sweep rate of 0.1 mV/s.

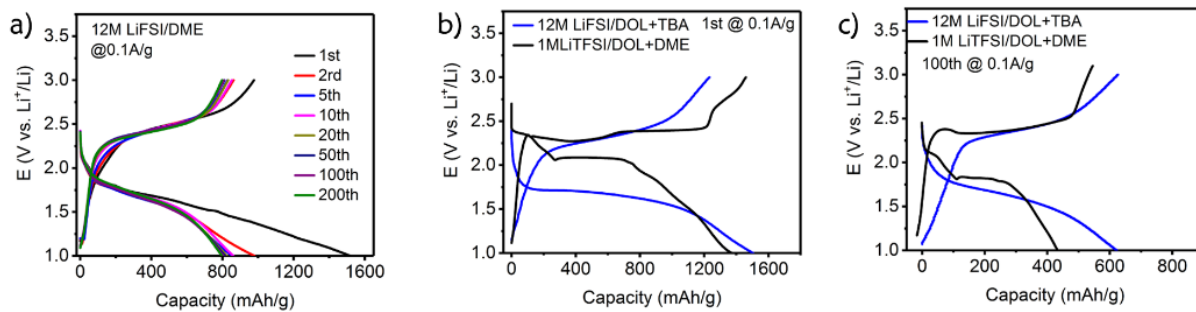


Figure S4. a) Charge-discharge curve at different cycles in 12M LiFSI/DME. A comparison of the charge-discharge curves at b) 1st and c) 100th cycle for a Li-S battery with different electrolytes.

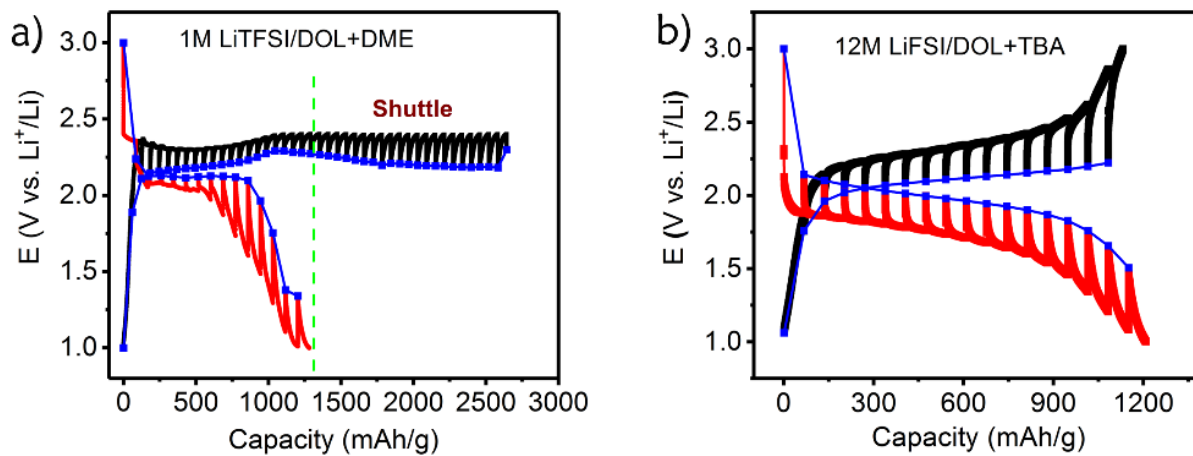


Figure S5. GITT curves in a) 1M LiTFSI/DOL+DME and b) 12M LiFSI/DOL+TBA electrolyte.

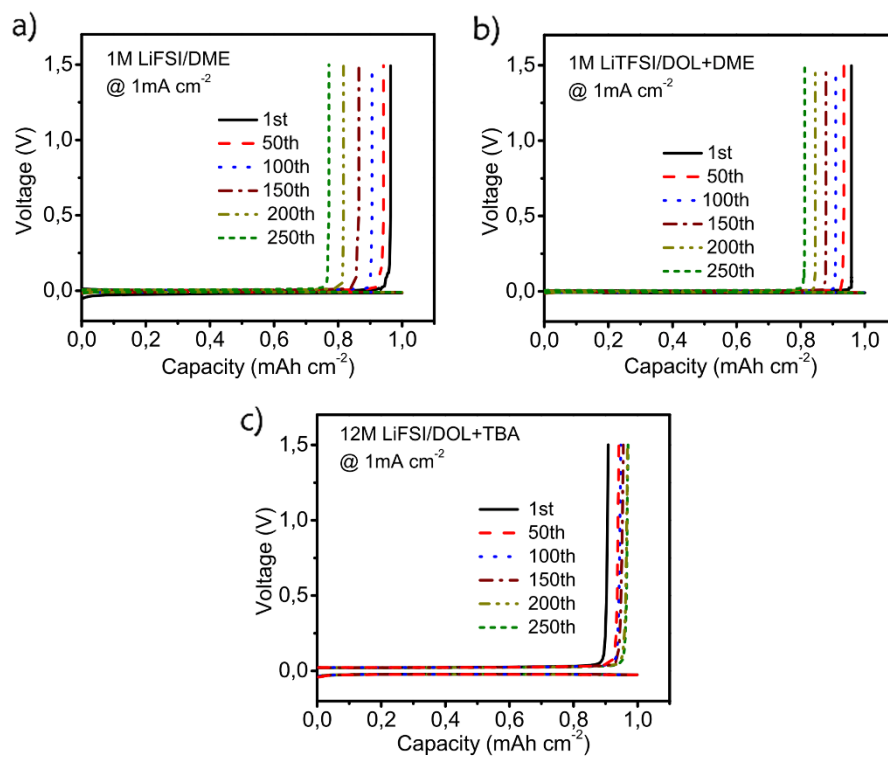


Figure S6. Voltage profiles of Li metal plating/stripping on Cu working electrode in a) 1M LiFSI/DME, b) 1M LiTFSI/DOL+DME, and c) 12M LiFSI/DOL+TBA with current of 1 mA cm^{-2} .

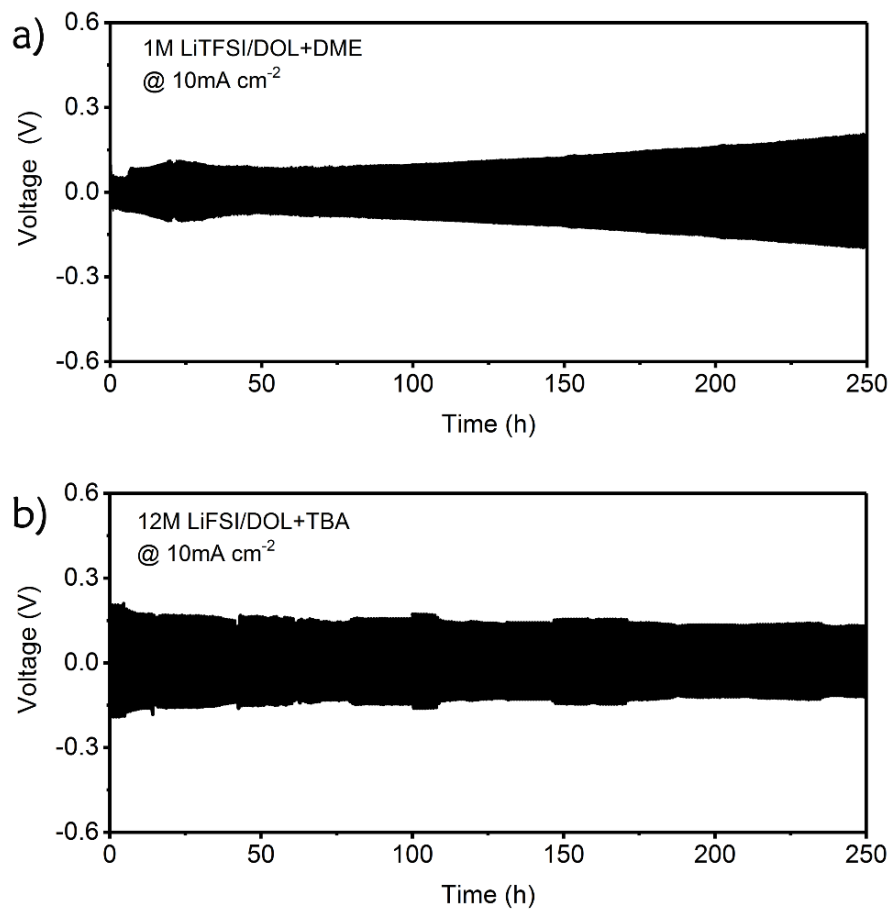


Figure S7. Voltage profiles during subsequent lithium plating/stripping processes from a Li|Li symmetrical cell at 10mA cm⁻² in a) 1M LiTFSI/DOL+DME and b) 12M LiFSI/DOL+TBA electrolyte.

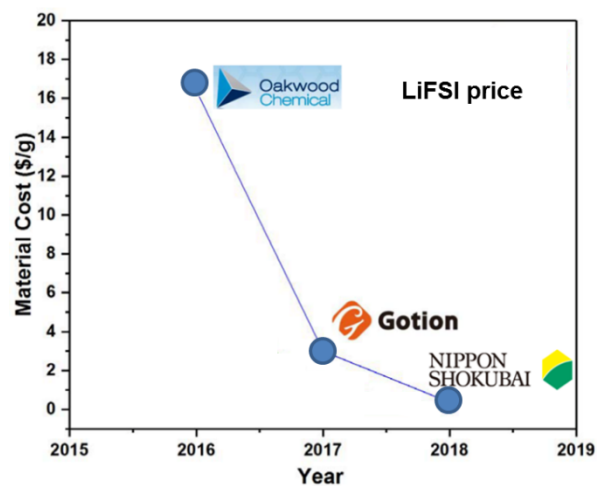


Figure S8. The variation of the LiFSI price in the past two years. In 2017, Gotion began to produce the LiFSI, the LiFSI price dropped from ~17 USD/g to ~3 USD/g. In 2018, another company (Nippon Shokubai) began to manufacture the LiFSI, which brings about further decrease of the price.